Indian Journal of Pure & Applied Physics
Vol. 60, February 2022, pp. 131-137

Effects of Al Content on Elastic Parameters of $Al_xGa_{1-x}As$ ($0 \leq x \leq 1$) Alloys

A Ouchtati[a], I Hadjoub[a, b], A Doghmane[a*], A Khoualdia[a] & Z Hadjoub[a]

[a]Laboratoire des Semi-conducteurs, Département de Physique, Faculté des Sciences, Université Badji-Mokhtar, Annaba, B.P 12, DZ-23000 Algeria

[b]Ecole Supérieure des Technologies Industrielles, ESTI, Annaba, DZ-23000, Algeria

Received 5 September 2021; accepted 14 January 2022

Elastic parameters of $Al_xGa_{1-x}As$ ($0 \leq x \leq 1$) alloys are numerically determined and analyzed on the basis of scanning acoustic microscopy technique. Thus, the dependence of Al concentrations, x, on all features of reflection coefficient and acoustic materials signatures (critical angles of reflected modes, spatial periods, peaks of FFT spectra and their corresponding wave velocities) has been considered, analyzed and discussed. It is found that as Al content increases several behaviors are obtained: (i) all critical angles of longitudinal, transverse and Rayleigh waves, decrease, (ii) all spatial periods increase and (ii) both Rayleigh and longitudinal wave velocities increase. Moreover, the variations of these parameters, P, were quantified and semi-empirical formulas were found to be of the form: $P = c + ax + bx^2$; from these formulas, valuable information can be derived and may be useful for $Al_xGa_{1-x}As$ compositional characterization.

Keywords: $Al_xGa_{1-x}As$, Elastic parameters, Acoustic microscopy, Acoustic signature, Reflection coefficient

1 Introduction

III-V Compound semiconductors and their ternary and quaternary derivatives are the basis of a wide variety of very interesting devices applied in several fields such as: metal-semiconductor field effect transistors, heterojunction bipolar effect transistors, high mobility field effect transistors for high speed data transmission networks, light emitting diodes for displays, information storage and communications, visible and infrared diodes, *etc*[1-5]. Thus, the engineering, processing and applications of heteroepitaxial thin films based on III–V compound semiconductors are of great importance in the fabrication of advanced electronic and optoelectronic devices for innovative power generation[6,7]. As a result of such interesting applications, it is becoming more important to characterize such crystals and to understand their fundamental properties. Thus, the growth of semiconductor mixed crystals, such as $Al_xGa_{1-x}As$, has attracted a great deal of attention due, in particular, to their good and ease of preparation via the established molecular beam epitaxial and liquid phase epitaxial methods[8].

Among control techniques or quality tests of materials, the non-destructive micro-characterization of elastic properties is not only crucial but also necessary for the quantification of the variations in elastic parameters. Moreover, any specific use of a material in the technological industry requires information on its mechanical characteristics. Therefore, the knowledge of elastic properties is suitable for describing the structure of materials according to their composition. These properties are related to various fundamental data of the solid state, such as inter atomic potential, equation of state, phonons spectra, specific heat, thermal expansion, Debye temperature and melting point[9,10].

The AlGaAs/GaAs heterostructures are considered as the most common choice to be used in many high speed and high frequency devices[11]. In fact, the characteristics of $Al_xGa_{1-x}As$ structures vary mainly with the composition, x. These alloys form the milestone of a great number of applications, such as: solar cells[12-14], photo-detector[15], spectroscopic avalanche photodiodes[16], single and double triangular quantum wells[17], terahertz quantum cascade lasers[18], high efficiency cathodes for photon-enhanced thermionic emission solar energy converters)[19], optical rectification coefficient of Thue–Morse multiple-quantum-well systems[20], etc. Moreover, the dependence of the Al composition on the properties of AlAs and GaAs semiconductor alloys is very important for various specific applications. For example, the design of the $Al_xGa_{1-x}As$ structure with a composition range varying from 0 to 0.45 produces

*Corresponding author: (E-mail: a_doghmane@yahoo.fr)

quality optical and electronic properties[13,21-23]. Whereas, the $Al_{0.7}Ga_{0.3}As$ composition shows more advantages for better choice in biodetection applications[24].

To enrich and complete these restricted composition values and unlike the endpoint values approach, we investigate the whole alloy composition $0 \leq x \leq 1$ in order to determine the elastic properties of the $Al_xGa_{1-x}As$ zinc-blende structure, at different fractions of Al. This large composition spectrum opens up more engineering pathways and optimizes the composition of this ternary material for specific technological applications. Our investigations were carried out using normal operating conditions of the dynamic and non-destructive technique of the scanning acoustic microscope, SAM, which is based on the emission and reflection of ultrasonic waves. It is worth noting that the SAM is a very promising tool for both qualitative and quantitative investigations of materials[25-29]; the results can be deduced either experimentally or theoretically. In the present work, making use of theoretical considerations, we study some elastic properties of $Al_xGa_{1-x}As$ ternary alloys and their dependences on aluminum molar fraction, *x*, in the whole range from $x = 0$ to $x = 1$. Thus, we first determine and analyze reflection coefficient, R(θ), as well as acoustic materials signatures, V(z). Then, we put into evidence the effects of Al composition on (i) incidence angles in R(θ), (ii) spatial periods, Gz, in V(z) signatures, (iii) Rayleigh velocities, V_R, and (iv) longitudinal velocities, V_L. Finally, we quantify these effects through the deduction of semi-empirical formulas giving the variation of such elastic parameters as a function of increasing *x* from 0 to 1.

2 Computational procedure

The calculation procedure consists of several steps: (i) calculating the reflection coefficient, (ii) computing the V(z) curves of the whole system specimen-lens from the angular spectrum model and (iii) deducing the velocity of the corresponding mode via Fast Fourier Transform, FFT, analysis. These steps are summarized below.

2.1 Reflection coefficient

The reflection coefficient, R(θ), provides valuable information on wave propagation in a material[30-34]; it is a complex function that admits a modulus, |R|, and a phase, φ. This coefficient depends on boundary conditions at the interface coupling liquid/solid specimen: acoustic impedance, Z, density, u, incidence angle, t, and different propagating modes. Thus, R(θ) should depict all critical angles at which each leaky mode is totally reflected at its own characteristic velocity. The R(θ) function, for acoustic waves, can be calculated by solving the acoustic Fresnel equation; it is given for a liquid/solid interface by:

$$R(\theta) = \left(Z_{sol} - Z_{liq}\right)/\left(Z_{sol} + Z_{liq}\right) \quad \ldots (1)$$

where Z_{sol} and Z_{liq} are solid and liquid impedances, respectively, they are expressed as:

$$Z_{sol} = \rho_{sol} V_L / \cos\theta_L \cos^2 2\theta_L + \rho_{sol} V_T / \cos\theta_T \sin^2 2\theta_T \quad \ldots (2)$$

$$Z_{liq} = \rho_{liq} \cdot V_{liq} / \cos\theta \quad \ldots (3)$$

where θ_L, θ_T, correspond to angles of total reflection of longitudinal and transverse modes, respectively, V_L and V_T are longitudinal and transverse velocities, respectively; ρ_{sol}, ρ_{liq}, V_{liq} are the solid, the coupling liquid density and propagating wave velocity in the liquid, respectively. In the evaluation of the reflection coefficient, a computer program was developed to carry out the necessary numerical calculations for different Al molar fractions.

2.2 Acoustic materials signatures

Acoustic materials signatures, also known as V(z) curves, represent the output response, V, as a function of the defocusing distance, z, when the specimen is vertically displaced towards the acoustic lens. Hence the V(z) response is the most important method for accurately determining materials surface velocities. Such signatures can be determined either experimentally via SAM techniques or theoretically from the angular spectrum model using Sheppard and Wilson formula[34]:

$$V(z) = \int P^2(\theta) R(\theta) \exp(2jkz\cos\theta) \sin\theta \cos\theta \, d\theta \quad \ldots (4)$$

where t is the angle between a wave vector (k) and the lens axis (z), $P^2(t)$ is the pupil function of the lens and $j = \sqrt{-1}$. The V(z) response, which is a periodic signal with a spatial period, Gz, was calculated for different Al molar fractions.

2.3 Rayleigh velocity

It should be recalled that the V(z) periodic signatures are the result of different interfering modes as well as the lens response. Therefore, its deduction

should be cautiously carried out by taking certain precautions. In fact, the computed V(z) curves represent the whole system specimen-lens. Therefore, the lens response $V_{lens}(z)$ should be eliminated. Hence, the spectral analysis treatment through fast Fourier transform, FFT, technique should only be applied to the real specimen response V_{sample} = V(z) - $V_{lens}(z)$. The obtained FFT spectra could consist of a single or several peaks. Consequently, from the sharp rays in the FFT spectra that correspond to characteristic periods, Gz, the propagating wave velocity values, V_C, can be precisely calculated according to[32]:

$$V_C = V_{liq}/\left[1 - (V_{liq}/2\,f\Delta z)^2\right]^{1/2} \quad \ldots (5)$$

where *f* is the operating frequency and the subscript c stands for Rayleigh, R, or Longitudinal, L, modes (c= R, L).The appearance of a given mode strongly depends on the SAM operating conditions: frequency, coupling liquid, opening angle of the lens, etc[27,29,34-36].

2.4 Simulation conditions

The present calculations were carried out under normal operating conditions of a scanning acoustic microscope in reflection mode: water couplant, an operating frequency, f = 140 MHz and a half-opening angle of the acoustic lens, θ_{lens} = 50°. It should be noted that under these operating conditions of a SAM, Rayleigh waves are the most dominant modes. Such waves are of great importance not only in surface defect detection, in nondestructive testing of materials but also in surface acoustic wave devices.

3 Investigation of GaAs elastic properties

Despite their importance, elastic properties of $Al_xGa_{1-x}As$ alloys are rarely investigated. In order to compute the acoustic parameters R+Ɛ, and V(z), according to Eq. (1-3), it is necessary to know the values of longitudinal and transverse velocities as well as the density of this alloy. In this case, we make use of the following relations given for a cubic zinc-blende structure in [111] direction[37-39]:

$$V_L(m/s) = 5400 + 790x + 260x^2 \quad \ldots (6)$$

$$V_T(m/s) = 2790 + 380x + 120x^2 \quad \ldots (7)$$

$$\rho\left(\frac{kg}{m^3}\right) = 5320 - 1560x \quad \ldots (8)$$

From these relations, it can readily be deduced that for x = 0: $(V_L)_0 = (V_L)_{GaAs}$ = 5400 m/s, $(V_T)_0 = (V_T)_{GaAs}$ = 2790 m/s and $(\mathfrak{u})_0 = (\mathfrak{u})_{GaAs}$ =5320 kg/m^3.

3.1 Reflection coefficient

Since the reflection coefficient is complex-valued function, we separately calculate its amplitude (modulus) |R(θ)| and its phase for the structure: water/GaAs. The obtained results for the amplitude are illustrated in Fig. 1(a). It can clearly be noticed that for total reflection , when the incident angle increases, the amplitude of the refection coefficient exhibits several features: (i) an initial saturation, (ii) a sharp peak corresponding to the longitudinal critical angle, θ_L = 16° (iii) another saturation, (iv) a smooth increase, which corresponds to transverse modes at θ_T = 32.5° and (v) a final saturation with $|R|$ = 1 corresponding to the case where no energy can be propagated.

The phase dependence on incidence angle is plotted in Fig. 1(b) for the same structure. As the incidence angle increases, the obtained curve also shows several fluctuations, as for $|R|$, occurring at the same critical angles at which different modes are totally reflectes: longitudinal, transverse and Rayleigh. It should be noted that the most important fluctuation, with $\Delta\varphi \approx 2\pi$ transition, occurs around the Rayleigh-wave critical angle (θ_R= 35.4°).

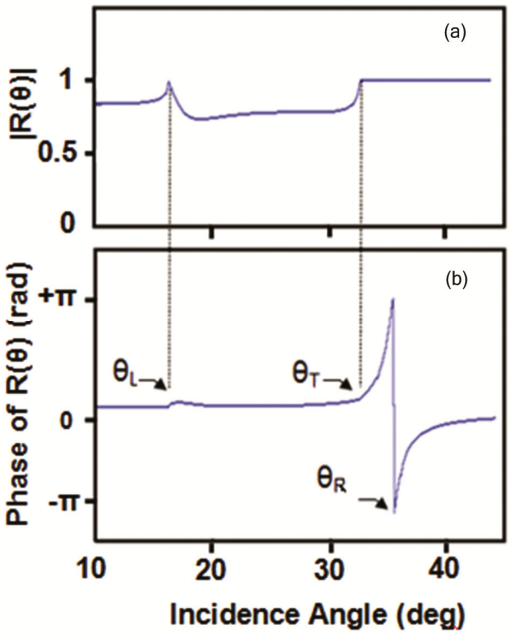

Fig. 1 — Variation of the amplitude (a) and phase (b) of the reflection coefficient as a function of the angle of incidence for the GaAs.

3.2 Acoustic signatures

The calculated acoustic signature of GaAs is illustrated in Fig. 2 in terms of the output signature as a function of defocusing distance, z. It can be seen that the curve exhibits an oscillatory behavior due constructive and destructive interference between propagating modes. This periodicity, with a spatial period, Gz, gives valuable information on surface acoustic wave, SAW, velocities involved in the interference phenomena. In the present simulation condition, Rayleigh mode is the most dominant one[29,31,32].

The signal treatment of this V(z) curve led via FFT technique to the spectrum shown in the insert of Fig. 2. The main peak corresponds to Rayleigh mode with a spatial period Gz = 29.3 μm. Therefore, from Eq. 5, it can be deuced that V_R = 2604 m/s. This value, though unknown in literature to the best of our knowledge, is physically acceptable since the Rayleigh velocity value is usually about 87 to 96% V_T [40] or about half that of longitudinal velocity.

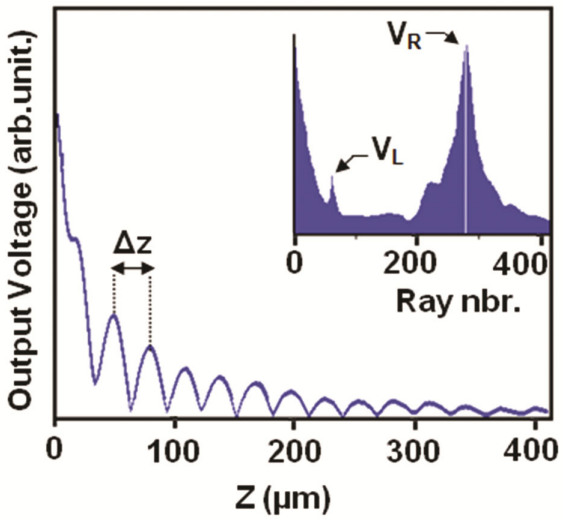

Fig. 2 — Acoustic signatures and FFT spectra of GaAs compound.

4 Study of elastic parameters of $Al_xGa_{1-x}As$ alloys

4.1 Effects of Al concentration on reflection coefficient

The influence of increasing molar fraction, *x*, on both phase and amplitude of reflection coefficient of $Al_xGa_{1-x}As$ structure is shown in Fig. 3 for some typical concentrations (*x* = 0; 0.2; 0.4; 0.6; 0.8 and 1).The curves are deliberately superimposed in order to put into evidence their differences. It can be seen that for the amplitude of the reflection coefficient Fig. 3(a), all the fluctuations, due to different mode excitations, observed above (in Fig. 1 for *x* =0), are also obtained with other different *x* values. The amplitude approaches unity beyond transverse modes as a result of total reflection with no transmitted energy in the $Al_xGa_{1-x}As$ sample. Moreover, as the molar fraction increases we notice that all critical angles (θ_L, θ_T and θ_R) shift towards lower values as regrouped in Table 1.

The influence of Al molar concentration on the phase of R(θ) of $Al_xGa_{1-x}As$ structure is illustrated in Fig. 3(b). We again obtain the same behavior as that described above for the amplitude with fluctuations at the same critical angles with an enhancement of the effect around Rayleigh modes and a less pronounced effect at longitudinal modes. Moreover, all the angle values shift towards lower incidence angles values from when *x* is increased from zero to unity.

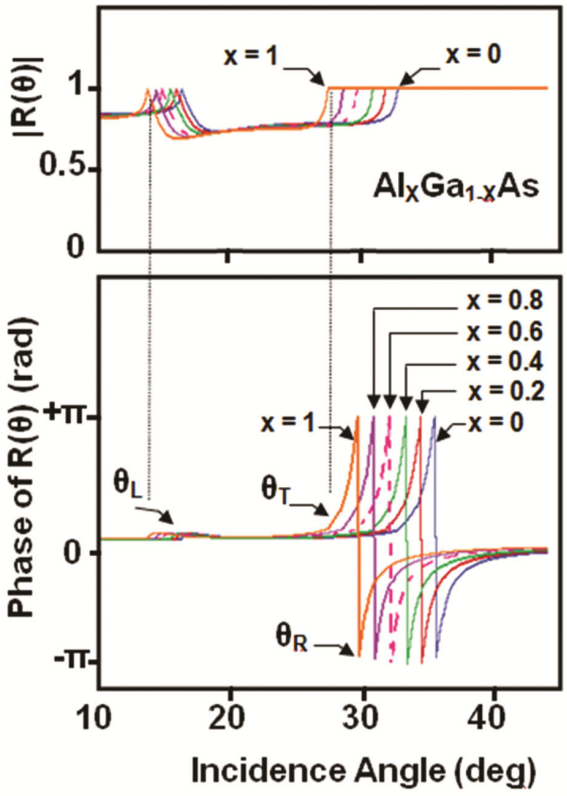

Fig. 3 — Variation of the amplitude and phase of the reflection coefficient as a function of the angle of incidence for the $Al_xGa_{1-x}As$ structure for $0 \le x \le 1$.

4.2 Effects of Al concentration on acoustic signatures

Acoustic signatures were calculated from relation (5) for $Al_xGa_{1-x}As$ structure at different Al molar fraction. The obtained V(z) curves are illustrated in Fig. 4 together with their respective FFT spectra for some typical concentrations (*x* = 0; 0.2; 0.4; 0.6; 0.8 and 1). For clarity, the V(z) curves normally superimposed were displaced upwards.

Table 1 — Deduced values of modes parameters of $Al_xGa_{1-x}As$

	Critical angles				Rayleigh mode		Longitudinal mode	
	θ_L (deg.)	θ_T (deg.)	θ_R (deg.)	Δz_R (μm)	V_R(m/s) from FFT	V_R (m/s) from Eq. 9	Δz_L (μm)	V_L (m/s) from FFT
x = 0	16.0	32.5	35.0	29	2604	2605	134.2	5364
x = 0.2	15.6	31.5	34.0	31	2679	2680	141.2	5511
x = 0.4	15.0	30.0	33.0	34	2759	2765	151.7	5694
x = 0.6	14.5	29.0	31.5	36	2867	2860	162.5	5885
x = 0.8	14.0	28.0	30.0	39	2965	2962	174.2	6097
x = 1	13.0	27.0	29.0	42	3080	3075	190.5	6370

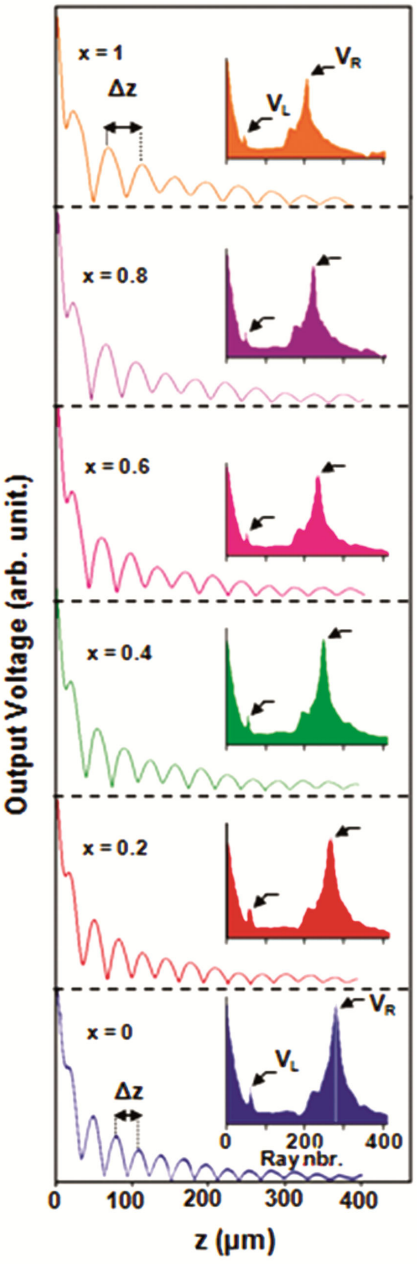

Fig. 4 — Acoustic signatures of $Al_xGa_{1-x}As$ compound at different Al concentration and their corresponding FFT spectra.

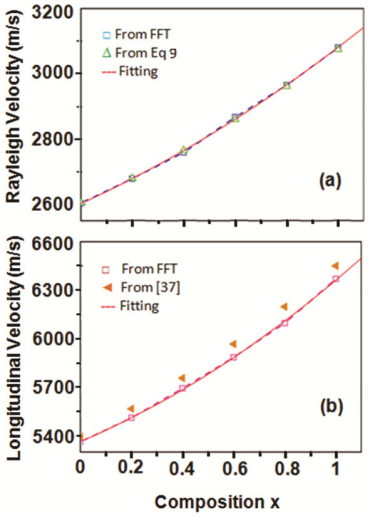

Fig. 5 — Rayleigh (a) and longitudinal (b) velocities of $Al_xGa_{1-x}As$ alloys at different Al concentrations.

It can clearly be seen that all V(z) curves show a maximum value at the focal point (z = 0 μm) followed by an oscillatory behavior with characteristic Gz periods due to constructive and destructive interference of different propagating modes[30-34]. However, as the aluminum concentration increases from 0 up to unity, we notice that the period Gz increases from 29 μm to 42 μm. These V(z) variations are better put into evidence via FFT spectra (inserts to Fig. 4) which show a clear shift of the principal ray towards higher spatial frequency values. Under the present simulation condition of normal operating SAM, the determined velocities correspond to Rayleigh propagation mode. It is found (Eq. 5) that as x increases from 0 to unity the Rayleigh velocity increases from that of GaAs (2604 m/s) to that of AlAs (3080 m/s).

4.3 Effects of Al concentration on Rayleigh and longitudinal velocities

To illustrate the effects of Al concentration on determined Rayleigh velocities, we plot in Fig. 5(a)

V_R as a function of *x*, presently calculated (Eq.5) from FFT spectra (ϒ ϒ ϒ). It is clear that as the Al concentration increases from 0 to 1 the Rayleigh velocity increases from that of GaAs to that of AlAs.

In order to, further, put into evidence this behavior, we adopt a second approach based on Viktorov formula[41] to calculate V_R:

$$V_R = V_T[0.718 - (V_T/V_L)^2]/[0.75 - (V_T/V_L)^2] \quad \ldots (9)$$

The obtained results, for every molar fraction from, are also plotted in Fig 5(a) (Δ Δ Δ); it can clearly be seen that the general tendency is for an increase of V_R as *x* increases. It should be noted that the agreement is quite good between both approaches. It is worth noting that, to our knowledge, there is no experimental investigation of such a behavior for Rayleigh velocities. The lack of reliable experimental data on the elastic properties of the system AlAs–GaAs is mainly caused by the difficulty to grow large high quality single crystals of these compounds[38]. A rare experimental result on elastic constants for the ternary $Al_xGa_{1-x}As$ (*x*=0.5) compound was carried out by the diffuse x-ray scattering[8].

To quantify the effects of Al concentration on determined Rayleigh velocities, we determined, through curve fitting in Fig 5(a) (——), the variations of V_R as a function *x*, for both approaches; the following polynomial dependence (solid curve) of the second order was deduced:

$$V_R(\mathrm{m/s}) = 2603 + 356.6x + 121.4x^2 \quad \ldots (10)$$

Thus, for *x* = 0 one obtains GaAs Rayleigh velocity, *i.e.*, $(V_R)_{GaAs}$ = 2603 m/s and for *x* =1 that of AlAs: $(V_R)_{AlAs}$ = 3081 m/s.

To enrich this investigation, we also determined longitudinal velocities from FFT spectra (shown in Fig. 4); the obtained results are plotted in Fig. 5(b) in terms of V_L as a function of x (ϒϒϒ). It can clearly be seen that the longitudinal velocity increases from that of GaAs (5364 m/s) to that of AlAs (6370 m/s) when the Al concentration increases from zero to unity. This behavior is very similar to that deduced from reported data[37-39] and represented by (◄◄◄) in Fig. 5(b). The similarities of V_R and V_L variations with Al concentrations are indicative of the same mechanism of SAW propagations. The quantification of V_L dependence on x gave a polynomial formula of the form:

$$V_L(\mathrm{m/s}) = 5377 + 664.571\,x + 317.857x^2 \quad \ldots (11)$$

The importance of this investigation lies in the direct determination, for a given Al concentration, of the exact desired acoustic wave velocity (V_R and V_L) by the application of the deduced Equations (10 & 11).

It should be noted that all investigated elastic parameters P (Gz, t_R, t_T, t_L, V_R and V_L) showed similar polynomial variations with Al content in $Al_xGa_{1-x}As$ ($0 \leq x \leq 1$) systems. These parameters were quantified and semi-empirical formulas were found to be of the form: $P = c + ax + bx^2$; from these formulas, valuable information can be derived and may be useful for $Al_xGa_{1-x}As$ compositional characterization. Moreover, if any of these parameters were determined by any other means, it would then be possible to deduce the exact Al concentration in the $Al_xGa_{1-x}As$ alloy.

5 Conclusions

In this work, based on the case of scanning acoustic microscopy simulations, we investigated the dependence of the Al composition on elastic properties of $Al_xGa_{1-x}As$ alloys with a composition range varying from 0 to 1. Hence, we first considered GaAs binary compound (from *x* = 0) then the effect of increasing Al content in up to AlAs (*x* = 1). In all cases, we calculated reflection coefficients from which critical angles of reflected modes: longitudinal, transverse and Rayleigh. Then, we deduced periodic acoustic materials signatures whose treatment and analysis led to the determination of spatial periods and consequently Rayleigh velocities. It was found that increasing the Al content from zero to unity led to several interesting results, such as:

- ✓ A decrease in the values of critical angles at which longitudinal, transverse and Rayleigh waves are totally reflected.
- ✓ An increase in spatial periods, in V(z) curves, from that of GaAs to that of AlAs
- ✓ An increase in Rayleigh and longitudinal velocities from that of GaAs to that of AlAs

Moreover, the quantification of parameter variation with Al content led to the deduction of similar polynomial which give valuable information that may be useful for $Al_xGa_{1-x}As$ compositional characterization; if any of these parameters is determined by any other means, it would then be possible to deduce the exact Al concentration of the investigated $Al_xGa_{1-x}As$ alloy and

vice versa. Moreover, it is worth noting that Rayleigh wave and longitudinal velocities are related to elastic constants through well-known formula. Thus, the dependence of V_R and V_L on Al content in $Al_xGa_{1-x}As$ alloys is of great importance in the determination of surface defects, stress deformation, shape recovery, modeling and parts design for electronic and optoelectronics devices.

Acknowledgments

This research work was supported by the DG-RSDT (MESRS), Algeria, under PRFU programs.

References

1 Fares F, Bouarissa N, Fares N E & Mezrag F, *Acta Physica Polonica A*, 137 (2020) 489.
2 Kawazu T, Noda T & Sakuma Y, *Appl Phys Lett*, 112 (2018) 072101.
3 Kilpi O P, Svensson J, Wu J, Persson A R, Wallenberg L R, Lind E & Wernersson L E, *Nano Lett*, 17 (2017) 6006.
4 Xie Z X, Yu X, Chen X K, Zhou W X, Shi Y M & Zhang L F, *Appl Phys Lett*, 116 (2020) 143102.
5 Swe H M T, Tun H M, & Latt M M, *J Nano Res Appl*, 8 (2020) 9.
6 Jeon N, Ruhstorfer D, Döblinger M, Matich S, Loitsch B, Koblmueller G & Lauhon L, *Nano Lett*, 18 (2018) 5179.
7 Pradhan A, Mukherjee S, Maitra T, Mukherjee S, Nayak A & Bhunia S, *Superlatt Microstruct,* 126 (2019) 193.
8 Kashiwagura N, Kashihara Y & Harad J, *Jpn J Appl Phys*, 25 (1986) 1317.
9 Ilchuk H A, Korbutyak D V, Kashuba A I, Andriyevsky B, Kupchak I M, Petrus R Y & Semkiv I V, *Semicond Phys Quant Electron Optoelectron*, 23 (2020) 355.
10 Boufadi F, Bidai K, Ameri M, Bentouaf A, Bensaid D, Azzaz Y & Ameri I, *Acta Phys Pol A,* 129 (2016) 315.
11 Filali W, Sengouga N, Oussalah S, Mari R H, Jameel D, Al Saqri N A, Aziz M, Taylor D & Henini M, *Superlayt Microstruct*, 111 (2017) 1010.
12 Sharbati S, Gharibshahian I & Orouji A A, *Solar Energy* 188 (2019) 1.
13 Liu L, Diao Y & Xia S, *Opt Commun*, 477 (2020) 126340.
14 Rana M M, Khan S M F & Shafayat M S, 1st International Conference on Advances in Science, Engineering and Robotics Technology (ICASERT), Brac University, Bangladesh, IEEE (2019).
15 Kumari B, Katti A & Alvi P A, International Conference on Emerging Trends in Communication, Control and Computing (ICONC3), Mody University of Science & technology, Lakshmangarch, India, *IEEE* (2020).
16 Whitaker M D C, Lioliou G, Krysa A B & Barnett A M, *J Appl Phys*, 128 (2020) 015704.
17 Zhao Q, Aqiqi S, You J F, Kria M, Guo K X, Feddi E, Zhang Z H & Yuan J H*, Physica E,* 115 (2020) 113707.
18 Flores Y V & Albo A, *IEEE J Quant Electron*, 53 (2017) 1.
19 Feng C, Zhang Y, Qian Y, Wang Z, Liu J, Chang B, Shi F & Jiao G, *Optics Commun*, 413 (2018) 1.
20 Solaimani M, *Eur Phys J Plus*, 135 (2020) 1.
21 Akura M & Dunn G, *Physica Status Solidi (b),* 256 (2019) 1800284.
22 Koudriavtseva O, Kudriavtsev Y, Escobosa A *&* Sánchez–R V M, 8th International Caribbean Conference on Devices, Circuts and Systems (ICCDCS), Playa Del Carmen, Mexico, *IEEE*, (2012).
23 Lal P, Dixit S, Dalela S, Rahman F & Alvi P A, *Physica E*, 46 (2012) 224.
24 Guerinik A & Tayeboun F, *Prog Electromagn Res Lett,* 92 (2020) 125.
25 Ida N & Meyendorf N, *Handbook of Advanced Nondestructive Evaluation*, Springer Nature Switzerland AG, (2019).
26 Maev R G, *Advances in Acoustic Microscopy and High Resolution Imaging*, Wiely-VCH Verlag, (2013).
27 Briggs G A D & Kolosov O V, *Advances in Acoustic Microscopy*, Oxford University Press, Oxford, (2010).
28 Yu Z & Boseck S, *Rev Modern Phys*, 67 (1995) 863.
29 Doghmane A, Hadjoub Z, Alami K, Saurel J M & Attal J, *J Acoust Soc Am*, 92 (1992) 1545.
30 Levy M, Bass H E & Stern R, *Modern Acoustical Techniques for the Measurement of Mechanical Properties*, Academic Press, London, (2001).
31 Doghmane A & Hadjoub Z, *J Phys D: Appl Phys*, 30 (1997) 2777.
32 Kushibiki J I & Chubachi N, *IEEE Trans Sonics Ultrason*, 32 (1985) 189.
33 Brekhovskikh L M, *Waves in Layered Media*, Academic Press, London, (1980).
34 Sheppard C J R & Wilson T, *Appl Phys Lett*, 38 (1981) 858.
35 Hadjoub Z, Doghmane A, Hadjoub F & Boumaiza Y, *J Mater Sci Lett,* 13 (1994) 759.
36 Hadjoub Z, Alami K, Doghmane A, Saurel J M & Attal J*, Electron Lett*, 27 (1991) 981.
37 Adachi S, *Properties of Aluminium Gallium Arsenide*, INSPEC IEE, London, (1993).
38 Krieger M, Sigg H, Herres N, Bachem K & Köhler K, *Appl Phys Lett*, 66 (1995) 682.
39 Adachi S, *J Appl Phys*, 58 (1985) R1.
40 Briggs A, *Rep Prog Phys*, 55 (1992) 851.
41 Viktorov L, *Rayleigh and Lamb Waves*, Plenum Press, New York, (1967).